

See discussions, stats, and author profiles for this publication at: <https://www.researchgate.net/publication/334981707>

High-Resolution Acoustic Emission Monitoring in Nanomechanics

Article in JOM: the journal of the Minerals, Metals & Materials Society · August 2019

DOI: 10.1007/s11837-019-03700-8

CITATIONS

15

READS

210

8 authors, including:



Radim Ctvrtlik
onsemi

84 PUBLICATIONS 928 CITATIONS

[SEE PROFILE](#)



Jan Tomastik
Palacký University Olomouc

55 PUBLICATIONS 666 CITATIONS

[SEE PROFILE](#)



Lukáš Václavěk
Palacký University Olomouc

161 PUBLICATIONS 1,795 CITATIONS

[SEE PROFILE](#)



B. D. Beake
Micro Materials Ltd.

200 PUBLICATIONS 6,101 CITATIONS

[SEE PROFILE](#)



High-Resolution Acoustic Emission Monitoring in Nanomechanics

RADIM CTVRŤLIK,^{1,2,5} JAN TOMASTIK,¹ LUKAS VACLAVEK,²
BEN D. BEAKE ,^{3,6} ADRIAN J. HARRIS,³
ALBERTO SANCHEZ MARTIN,³ MICHAL HANAK,⁴
and PETR ABRHAM⁴

1.—Institute of Physics of the Czech Academy of Sciences, Joint Laboratory of Optics of Palacký University and Institute of Physics AS CR, Olomouc, Czech Republic. 2.—Regional Centre of Advanced Technologies and Materials, Joint Laboratory of Optics of Palacký University and Institute of Physics of Academy of Sciences of the Czech Republic, Faculty of Science, Palacký University, 17. listopadu 12, 77146 Olomouc, Czech Republic. 3.—Micro Materials Ltd, Willow House, Yale Business Village, Ellice Way, Wrexham LL13 7YL, UK. 4.—ZD Rpety - Dakel, Ohrobecká 408/3, 142 00 Prague, Czech Republic. 5.—e-mail: ctvrtlik@fzu.cz. 6.—e-mail: Ben@micromaterials.co.uk

In many cases, the load–depth–time record in a nanomechanical or nanotribological test does not provide sufficient information, and subsequent microscopic imaging does not directly provide information on the dynamics of the process being studied. Analysis of the acoustic waves generated during these tests can overcome this drawback and offer a non-destructive way for obtaining complementary information. Acoustic waves emitted during mechanical tests at the nano/micro scale are a rich source of information about the deformation behavior that can otherwise be inaccessible by traditional methods. Analysis of acoustic emissions (AE) can provide a better understanding and more complex interpretation of nanomechanical and nanotribological results even at the nano/micro scale. In this study, the strength of an AE-based method is demonstrated for various types of materials, including hard SiC coatings, silicalite-1 zeolite microcrystals, Fe₃Si bulk and partially stabilized zirconia explored using nano-indentation, nano-scratch tests and repetitive nano-impact tests.

INTRODUCTION

The research and development of new materials are inherently related to the quality of information that can be obtained experimentally. A variety of experimental techniques, both quasi-static and dynamic, have been introduced for the exploration of nanomechanical and nanotribological properties at room temperature as well as at elevated temperatures.¹ Although these techniques and their analysis protocols are well established and have been used for years for testing of thin films and bulk materials, the information provided by these tests can be dramatically enhanced by acoustic emission (AE) detection systems even at the nano/micro scale.^{2–4} As a result, more reliable conclusions about the material performance can be obtained. The initial stages of plastic deformation or cracking can

be in situ monitored, providing detailed information on the dynamics of the deformation process. Acoustic emission can be defined as the phenomenon of transient elastic waves radiation in solids that occurs when a material undergoes irreversible changes in its internal structure, or in other words during a dynamic reconstruction of the material's structure that is represented mainly by crack formation, plastic deformation or phase transformation, etc. Typical plastic deformation-related phenomena include twinning, activation of dislocation multiplication sources or activation of pre-existing dislocations.⁵ Unlike the above-mentioned material AE, mechanical AE is mechanical in origin and refers to processes such as friction, impact, etc. Generally, mechanical loading of a material can result in structural changes and in turn to the generation of elastic stress waves. Consequently,

small surface displacements of a material can be detected. This effect is especially strong when the accumulated elastic energy is released rapidly from a localized source. In practice, the AE method is based on the mechanism described above and has been used, for example, for structural health monitoring, quality control, system feedback, process monitoring, etc.

AE monitoring is conventionally employed for exploring the interfacial and cohesive failures of large-scaled objects. Since the energy released during these tests is much higher in comparison to the highly localized volumes in nanomechanical and nanotribological tests, AE sensors with optimized design have to be used to achieve sufficient sensitivity and reliability. In all of these tests, micromechanical contact between the surface under investigation and the defined counter-body is introduced. Three different approaches to monitor the AE signals generated during the test have been introduced. Originally, standard sensors used for large-scale testing have been employed for exploring fracture⁶ and plastic instabilities^{7,8} of thin films and coatings,^{9–11} bulk materials^{6,7} and interfaces.¹² Despite their easy experimental implementation with suitable coupler (glue, wax, vaseline, etc.) and direct attachment to the sample, large-scale sensors do not provide sufficient sensitivity. This may be related to the non-optimized design for low-energy AE events (internal noise level, low band width, long rise time, etc.) occurring during mechanical tests at the nano/micro scale. The AE sensor placement also has to be considered to not interfere with the indenter and/or to not unduly affect the mechanical compliance of the loading frame. Another approach is based on the proper coupling of the AE sensor directly to the indenter,¹³ where the AE signal is directly sensed in the vicinity of the contact area. Finally, dedicated sample holders with inbuilt AE sensors with optimized design also featuring high mechanical stiffness can be utilized.^{14,15} Due to their advanced design with improved sensitivity and extremely low noise, these are well suited for routine use in nanomechanical test instruments.

In the following sections, we explore the use of advanced AE to study diverse phenomena in different materials in various nanomechanical setups, such as plastic instabilities in Fe₃Si single crystals during spherical indentation, cracking of hard coatings during indentation and scratch tests, quasi-static crushing of microcrystals, and dynamic impact testing of partially stabilized zirconia. In all these examples, the benefits and features of utilizing AE monitoring are outlined.

INSTRUMENTATION

Nanomechanical tests were performed using a calibrated NanoTest system (Micro Materials, Wrexham, UK) instrument at room temperature

with diamond indenters. Nano-indentation and scratch tests were performed with Rockwell spherical indenters with different radii. The internal integrity of the zeolite crystals was also tested with Berkovich and Cube-corner indenters, and repetitive impact testing was performed with a cube-corner indenter. AE activity was continuously recorded and analyzed during the whole test using the high-sensitivity ZEDO system (Dakel, Prague, Czech Republic) which has a high dynamic range and a sampling frequency of 10 MHz, enabling the study of very weak as well strong AE events at the nano-/micro-second scale in a broad frequency range up to 2 MHz. With direct synchronization with the nano-indenter, the depth–load–time records can be related to the AE signal. Continuous recording of the AE signal is very important for subsequent analysis and interpretation.¹⁴ During the test, the samples were mounted on low-noise/high-sensitivity AE sample holders employing a dedicated structured piezo-element and inbuilt pre-amplifier. The design of the sample holder reflects the need for mechanical robustness, simple manipulation and universal utilization in any nano/micro-indentation or tribological system (see Fig. 1). The samples were fixed using special low melting point wax or superglue.

In theory, two types of AE emission can be distinguished, as shown in Fig. 1b. A burst emission, characterized by discrete wave packets, is generated by separate AE events, while continuous emission is the result of the superposition of many small AE events. The AE hit waveform sampled at MHz frequency is described by several characteristics that provide different insight into the origin of detected signal (see Fig. 1c). Signal amplitude is related to the intensity of the AE generating event (cracking, plastic deformation, phase transition, delamination, debonding, friction, etc.). The energy of the signal provides information about the extent of the AE event and is calculated as the area under the squared signal envelope. The hit rise time is defined as the time between the beginning of the hit and the time of AE amplitude maximum, and may be used for the estimation of the lifetime of the physical event generating elastic strain waves. The rise time should be considered only as the upper bound of the event lifetime, as it is affected by a variety of factors like sensor characteristics, signal reflection, etc.⁷ Another popular approach to quantify AE activity is by the number of “counts”, which are defined as the number of times a signal crosses a pre-defined threshold. Due to the very high sampling frequencies, the signal envelope for a specific time period are averaged and presented as a compressed overall signal envelope to provide a visual overview of the AE signal as a function of time (see Fig. 1b). The signal RMS (root mean square) is also often used and provides direct information about the energy of the signal, but very

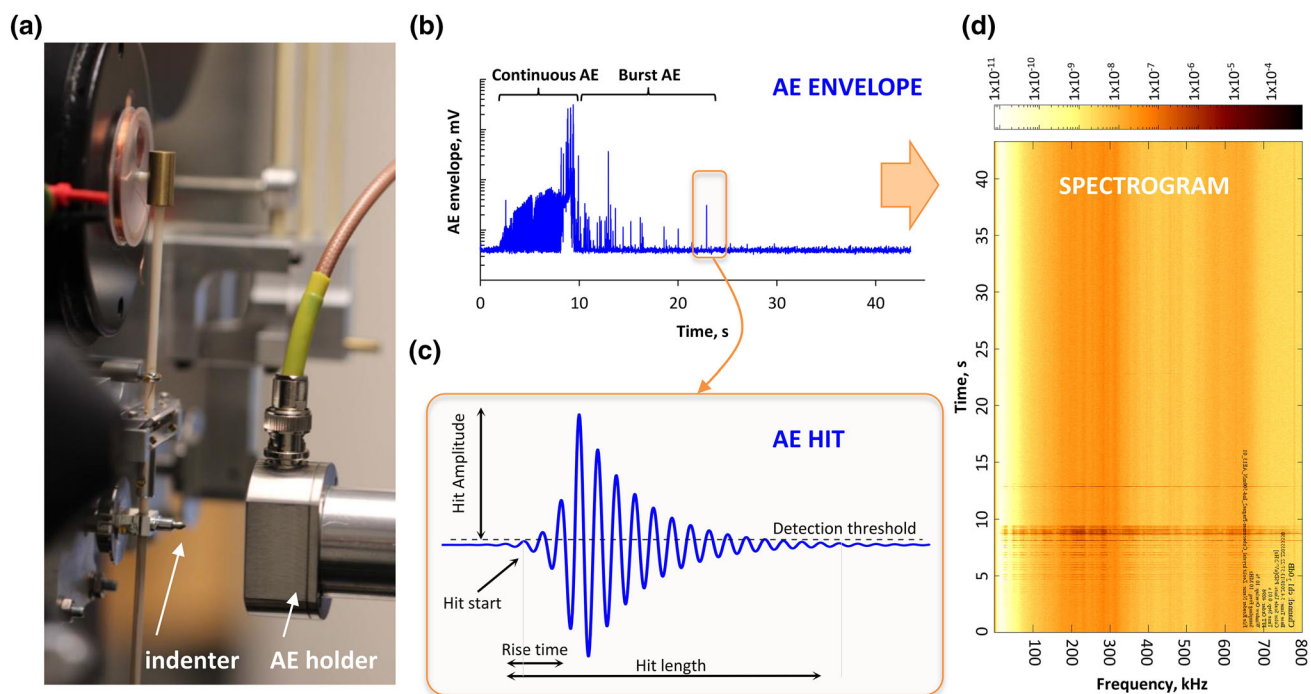


Fig. 1. (a) Acoustic emission holder implemented in the NanoTest system, (b) AE envelope (compressed signal), (c) AE hit waveform (full resolution signal) and (d) spectrogram corresponding to the crushing of the silicalite-1 zeolite crystal by a cube-corner indenter (see Fig. 3).

fast and low-energy events may not be distinguished. Although in most cases the AE signal is analyzed in the time domain, it has been noted that advanced frequency analysis (see spectrogram in Fig. 1d) may offer distinct advantages and provide deeper insights into the localized physical processes taking place during plastic deformation or cracking. For example, new strategies have been proposed to distinguish between different dynamic processes taking place during the mechanical contact.^{3,16,17} Generally, the AE signal and its characteristics are affected by the detector and the dimensions of the sample, so that direct comparison of absolute values between various studies is problematic.^{7,16} Nevertheless, the detection and analysis of AE signals provide a very reliable experimental approach for phenomenological exploration of the above-mentioned phenomena provided a single sensor is used in a given study.^{7,13}

Although the AE technique is particularly suitable for brittle materials, where AE signals with higher intensity are detected, ductile materials can be tested provided the AE signals can be detected over the background noise. The extremely low noise-floor sensor design implemented in the current setup may have applications in testing more ductile materials, where AE signals have been reported as low-amplitude wide-band noise-like high-frequency range signals.¹⁷ In addition, the yield-related phenomena and phase transitions can be advantageously explored via AE even in ductile materials.¹⁸

ONSET OF PLASTIC FLOW

During the initial stages of nano-indentation experiments the diamond tip penetrates into the surface elastically. Upon reaching the yield point where either von Mises or Tresca criteria for the resulting (applied) shear stresses are fulfilled, the plastic deformation starts to contribute to the total deformation. With a sharp pyramidal Berkovich or cube-corner indenter, the transition from an elastic to an elasto-plastic regime takes place during the very first stages of indentation. In contrast with spherical indenters, the plastic strain gradually grows with increasing contact pressure as the yield point is exceeded, resulting in smooth indentation curves.¹⁹ Nevertheless, oxide film breakage,²² film-substrate delamination,¹² phase transformation and/or different types of plastic instabilities, such as dislocation slip or twinning, can lead to discontinuities on the loading curve,^{20–22} and not only in bulk single-crystal materials.^{23,24} The onset of plasticity in load-controlled nano-indentation may be represented by sudden displacement bursts on the indentation curve, often called pop-ins. These depth-load discontinuities are related to the activation of slip and/or nucleation of dislocations and occur when the shear stresses are of the order of the theoretical strength.^{23,25} This phenomenon is more common in relatively defect-free solids with a low density of dislocations and their multiplication sites.²³ Before the pop-in event, i.e., before the initiation of plasticity driven by homogeneous dislocation nucleation and/or dislocation

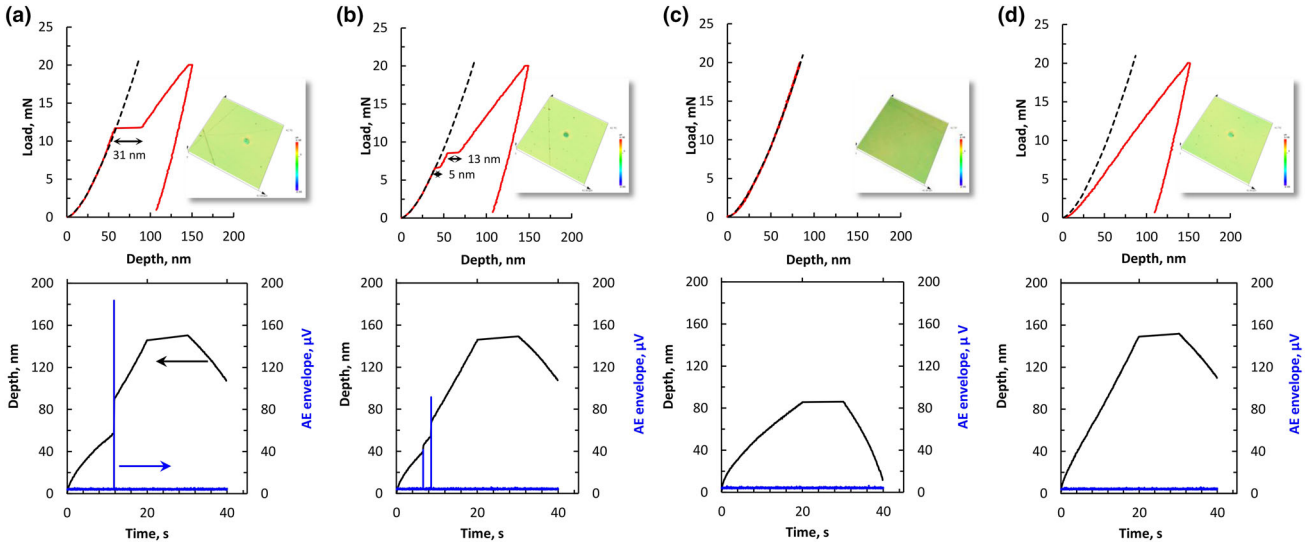


Fig. 2. Typical indentation curves with corresponding AE envelopes and images of residual indents. (a) Single AE event correlating with displacement step, (b) two AE events and displacement steps, (c) fully elastic contact without AE and (d) gradually developing plasticity without AE. Dashed line elastic Hertz contact (Eq. 1).

multiplication, the material supports elastic loading which approaches the applied shear stresses of the order of the theoretical shear strength of the material.^{26–28} Following the Hertz elastic contact theory,^{29,30} the initially purely elastic loading $P = P(h)$ can be generally described by:

$$P = \frac{4}{3} E^* \sqrt{R h} \quad (1)$$

where P denotes the normal indentation load, h is the penetration depth, R is the indenter radius and E^* is the reduced modulus,²⁹ taking into account the elastic deformation of the indenter ($1/E^* = (1 - \nu^2)/E + (1 - \nu_i^2)/E_i$, where ν , ν_i and E , E_i are Poisson's ratios and Young's moduli for the sample and indenter, respectively). Before pop-in, the load–displacement curve is reversible and well described by the Hertz equation, so no residual indent is formed on the surface.³¹

For the current study, the body centered cubic Fe3Si single crystal was chosen as a model ferritic iron-based alloy material for exploring the yield phenomenon during indentation loading.^{5,7} The Fe-Si(3 wt.%) single crystal was prepared by the floating-zone melting technique. Then, the sample with dimensions of 5 mm × 10 mm × 2 mm was cut so that the $\langle 100 \rangle$ direction was perpendicular to its surface. Standard mechanical grinding and polishing steps were followed by electrochemical polishing to prepare a suitably stress-free surface. Nano-indentation experiments to 20 mN were carried out with a spheroconical indenter with actual tip radius of 8500 nm. The sample was indented in the $[100]$ direction to 20 mN at 1 mN/s, with 10 s at this load, before unloading at 2 mN/s. The spherical indenter was used due to its inherent absence of geometrical similarity, so that the transition from a purely elastic to an elastic–plastic regime could be

conveniently explored. Typical indentation curves (Fig. 2) exhibit all possible scenarios ranging from transient elastic–plastic transition occurring almost at the very beginning of loading through sudden development of plastic deformation associated with pop-ins to purely elastic behavior. Discontinuities in penetration depth at constant load (pop-ins) can be defined by the critical load P_c and excursion depth Δh . Up to two distinct pop-ins were observed that coincided with the AE signal. This “staircase”-yielding character may be related to the activation of different slip systems and/or a limited number of particularly oriented slip systems in interaction volume. A clear relationship between the pop-in length and the AE envelope amplitude was observed. Due to the very high sensitivity of the AE setup, excursions as small as 3 nm can be detected and clearly identified in the AE envelope. In some cases, smooth indentation curves with immediate plastic were also observed. In these cases, right from the beginning of the indentation process, the indentation stress field interacts with pre-existing dislocations, slip is activated, and other dislocation sources are generated that in turn lead to dislocation multiplication and their interaction, resulting in continuous plastic deformation. In other tests, totally elastic load–depth curves without any discontinuities or residual indentation were obtained. Since no dynamic reconstruction of the crystal lattice takes place in these two cases, no AE signal was detected.

Fitting the loading curve with the Hertzian elastic model ($E^* = 210$ GPa measured via nano-indentation) shows good agreement with the purely elastic experimental curve (Fig. 2) and with the initial portions of the other loading curves, implying purely elastic behavior before the pop-in occurs. The onset of plasticity may be related to pop-ins and is

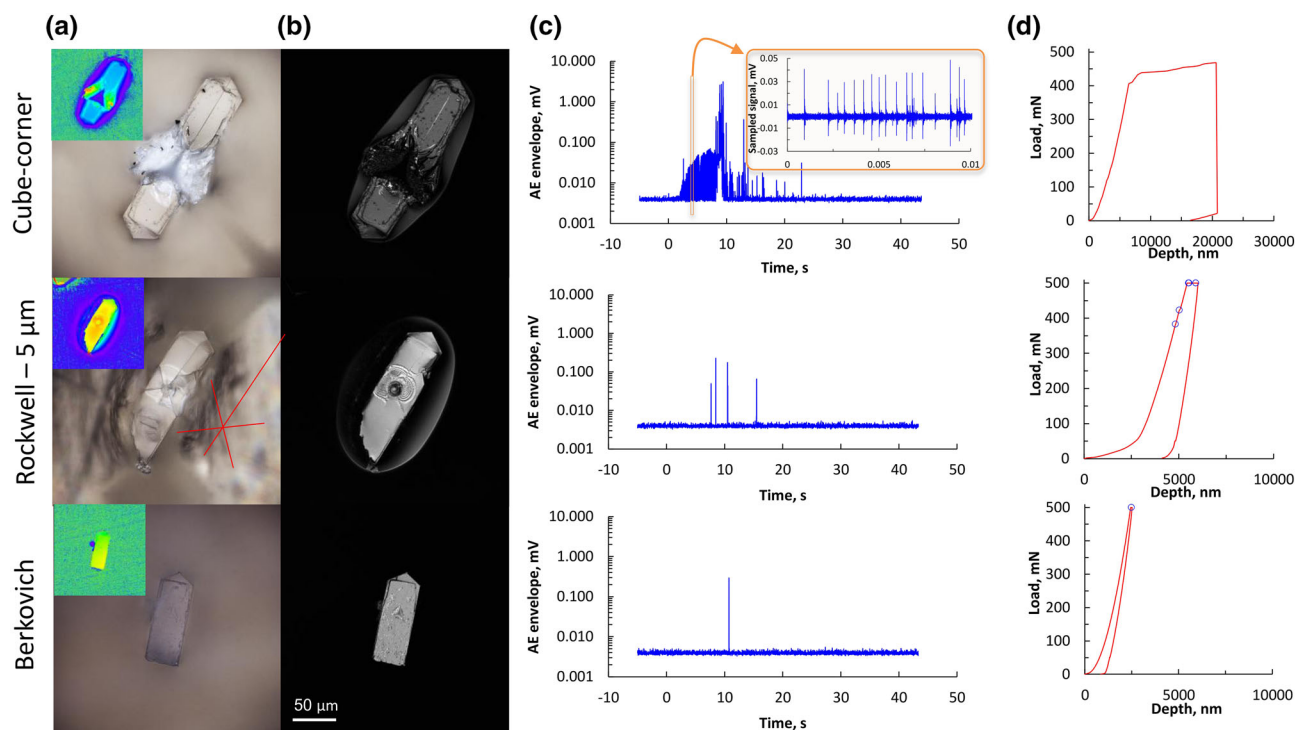


Fig. 3. Residual indent images: (a) bright light, (b) single wavelength intensity image (405 nm) with corresponding (c) AE envelopes and (d) indentation curves. Inset shows very intensive burst AE emission; as a result, the AE envelope shows a continuous character; open circles indicate the occurrence of AE events on the indentation curves.

believed to be associated with the dislocation nucleation and/or slip activation, especially in relatively defect-free materials.⁸ After slip activation, the plasticity results in deviation from the Hertz model.

CRACKING OF MICROCRYSTALS

Although AE developed as a non-destructive macroscopic method, it can also be utilized for exploration of deformation behavior of microscopic objects like microcrystals or microparticles. With a proper experimental setup and under appropriate experimental conditions, micro-objects with sizes ranging from several tens of microns can be conveniently tested. Individual objects as small as $40 \times 40 \times 200 \mu\text{m}$ can be explored using AE during load-controlled nano-indentation experiments.³² Silicalite-1 zeolite crystals grown by hydrothermal synthesis were indented to 500 mN along their [010] (b-axis) with Berkovich, Cube-corner and 5- μm end-radius spheroconical indenters. The different indenter geometries were used in order to explore the critical properties of the crystals and understand the deformation response that are of fundamental importance in areas like separation membrane production^{33,34} or crystal micronization.³⁵ In the latter case, the resistance against crack formation

and propagation is of great importance in the pharmaceutical industry, as it determines the degree of size reduction during comminution.³⁶

Typical crack patterns with a corresponding AE envelope for crystals indented with different indenters are shown in Fig. 3. With the Berkovich indenter, a plastic residual indentation without distinguishable cracks can be observed, while the AE record hints at some subsurface cracking. The cube-corner total crushing of the crystal was observed with an almost continuous AE envelope. A closer look at the indentation curve and the AE envelope reveals that the crystal was able to withstand inner cracking until its catastrophic disintegration at a load of approx. 400 mN. After spherical indentation, a typical crack pattern can be observed. Taking the silicalite-1 framework structure consisting of intersecting zig-zag (along [100]) and straight (along [010]) channels, it may be concluded that the crystal cracks preferentially along the straight channels. It should be noted that the porosity of the silicalite-1 crystals can be estimated as 30% due to the presence of these channels.³² Although the AE envelope shows a continuous character, the sampled signal reveals very intensive bursts of AE reflecting the sequence of cracking, see inset in Fig. 3. The corresponding

spectrogram showing visual representation of the spectrum of frequencies of the AE signal as a function of time is shown in Fig. 1d.

CRACKING IN HARD COATINGS

At a first consideration, it could be assumed that the AE signal should be monitored only during the mechanical or tribological testing, when the probe is in mechanical contact with the sample. However, various types of cracks may be formed depending on the actual state of the stress field under the indenter and material type. For example, median cracks are commonly formed during loading when the indenter is penetrating the material, while lateral cracks are formed during unloading.³⁷ These lateral cracks may continue to grow even after unloading, so it is necessary to always monitor the AE signal for at least several seconds after complete unloading.

A typical example of this behavior occurs in the indentation of a brittle SiC hard coating ($H = 33$ GPa) magnetron-sputtered onto a Si substrate (see Fig. 4). In this case, the coating was elastically loaded twice up to 250 mN during a multiple load–unload experiment, with partial unloading to 75 mN with an 8500-nm end-radius spherical indenter; the loading cycle is depicted by the green line in Fig. 4b. Despite the purely elastic and smooth character of the indentation curve (Fig. 4a) a characteristic crack pattern was revealed during subsequent microscopic observation. The elastic behavior was confirmed by repeated loading: compare the indentation curve in Fig. 4a and the penetration depth–time record (black line in Fig. 4b). Although the indentation curve does not provide any information about cracking, the AE envelope clearly shows that strong AE events occurred after complete unloading. Since the AE envelope (blue line in Fig. 4b) is a compressed signal, it does not directly provide detailed information about the process dynamics. Nevertheless, the 5-MHz sampled signal shown in Fig. 4c clearly reveals the formation of cone and through-thickness cracks typical for this type of coating.¹⁵

NANO-SCRATCH TEST

The instrumented scratch test is a common method for the evaluation of adhesive–cohesive properties of film–substrate systems.³⁸ Various deformation and failure modes may occur during the scratch test, including ploughing, tensile cracking, brittle film cracking and film delamination, according to the mechanical properties and the adhesion of the studied film–substrate system.³⁹ Scratch test evaluation is based on the accurate identification of the onset of deformation or film failure, based on microscopic observation of residual scratches and/or the analysis of the depth change record, but this approach can meet its limit in specific film–substrate systems.⁴⁰ For example, in

the case of opaque film, initial cracks may occur first at the film–substrate interface or in the substrate itself without observable traces on the film surface or on the depth–load record. At the same time, it may be very difficult to distinguish between adhesive and cohesive failure in the film–substrate system.⁴¹ One solution is to implement AE monitoring alongside these traditional evaluation techniques. The AE signal can thus be compared to the microscopic image of residual scratches, providing more accurate information about failure modes as well as improved understanding of the failure dynamics not possible by traditional methods.^{14,42} Deeper insight into the coating–substrate deformation and cracking modes can be obtained using an advanced analysis of large amounts of AE data and by the introduction of modern approaches, such as neural networks or by frequency analysis.^{3,16,17,43,44} To illustrate the advantages in using AE in scratch tests, magnetron-sputtered amorphous SiC films deposited on silicon substrates are used as a model material. The scratch test was performed with a 5- μm spheroconical indenter over a 450- μm track up to 500 mN. The images of residual scratches for the as-deposited and 900°C vacuum-annealed SiC films are shown in Fig. 5 along with the AE envelope. The as-deposited film shows a plastic residual groove with small surface cracks initiating at the end of the track (~ 40 s), while the marked AE signal can already be observed at ~ 25 s. Despite the fact that the as-deposited SiC film shows high scratch resistance and toughness, the first cracks initiated in the substrate long before cracks were observed on the surface of the film. AE monitoring improves the accuracy of determining the initial failure in the studied system, which was undetectable by other methods. The AE envelope shown in Fig. 5 is a compressed signal that provides a quick overview of the AE activity during the test. In order to analyze the individual AE events, the sampled signal of the AE signal is actually a sequence of discrete AE events that can be depicted in full time resolution as the so-called “hits”. Such hits can be further analyzed in terms of their individual energy and time parameters.

Extended analysis of the AE signal can be shown on a second sample of SiC film annealed at 900°C under vacuum (see Fig. 5). Annealing led to increased brittleness which resulted in the occurrence of faint surface angular cracks at ~ 9 s and initiation of the longer and wider angular cracks propagating far outside the residual groove beyond 15 s. The AE envelope correlates with visual observation in term of cracking onset detection as well as cracking intensity. After failure, the AE amplitude for the annealed film is significantly higher than the as-deposited film. Total failure of the film is identified at ~ 27 s where pronounced film and also substrate cracking and spallation starts. Cracking of the Si substrate may be responsible for the observed AE amplitude increase, and then

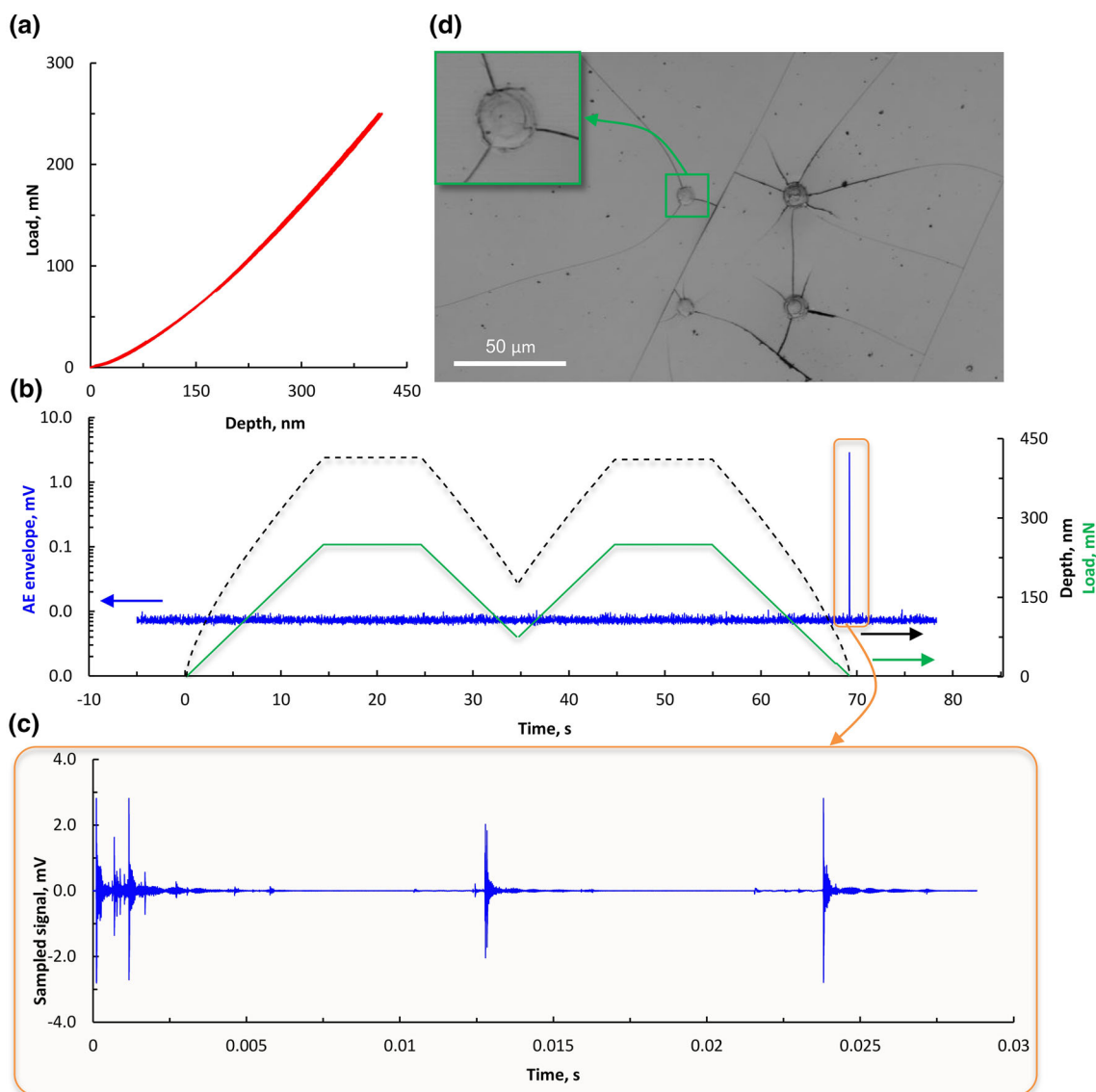


Fig. 4. Spherical indentation into the SiC thin film on silicon: (a) purely elastic indentation curve. (b) AE envelope (blue), indentation load (green) and depth (dotted black line) as a function of time, (c) AE bursts in full resolution representing the peak in the AE envelope, and (d) residual indents with apparent cracking (Color figure online).

significant breaking of the film proceeds. Direct correlation between the extent of cracking and the AE parameters can be seen in Fig. 5, where it is shown that longer hits possess higher energy. A decrease in hit energy at ~ 33 s may be explained by the breaking off of a large portion of the substrate in front of the moving indenter, after which further material cracking is temporarily reduced. Subsequently, the locally persisting film protects the substrate from breaking off in the plateau area, and in turn leads to a decrease of the detected AE signal.

NANO-IMPACT TESTS

Nano-indentation can be used to assess toughness as a measure of resistance to crack initiation and overload failure, but it is not possible to

monitor crack propagation under repetitive, oscillating loading conditions in the standard quasi-static nano-indentation test. The dynamic, high-strain-rate repetitive nano-impact test is a suitable alternative. The high-strain-rate contact in this test can provide much closer simulation of the performance of coating systems under highly loaded intermittent contact and the evolution of wear under these conditions. Although hard PVD coatings fail the nano-impact test at high load when sharp cube corner probes are used, when blunter probe geometries are used, it is not usually possible to cause rapid fracture on these types of samples.^{45,46}

In the following example, the performance of two technical ceramics has been evaluated under repetitive impact with AE using a spheroconical probe,

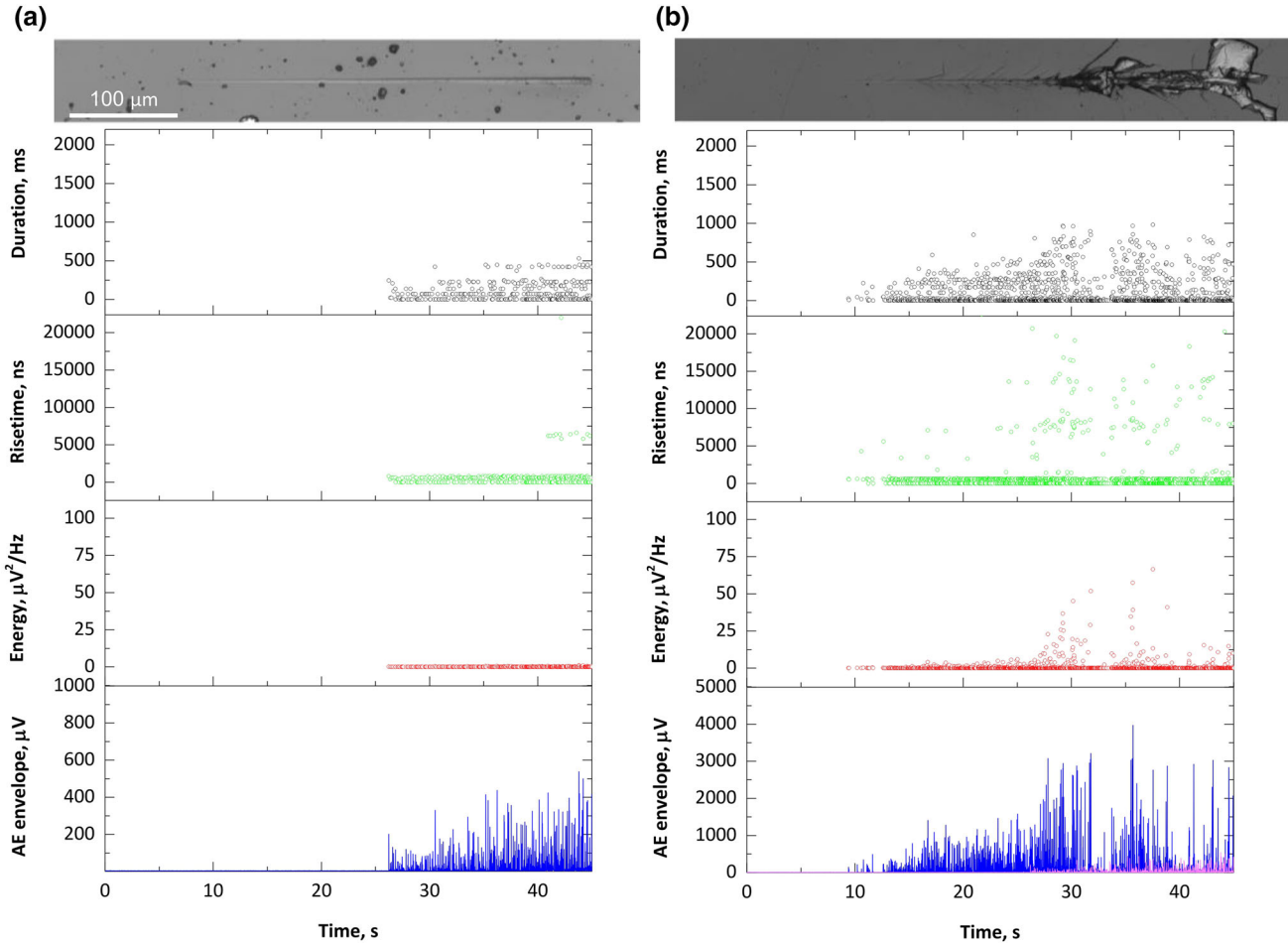


Fig. 5. Advanced scratch test evaluation for (a) as-deposited and (b) 900°C vacuum-annealed SiC film on a Si substrate. Microscopic images of residual scratches are followed by various parameters of AE hits: length, rise time, energy and AE envelope. The envelope for the as-deposited film (pink) is shown together with the envelope for the annealed film for direct comparison (Color figure online).

and under very low load with a sharp probe to investigate the influence of probe geometry on the damage progression mechanisms. Nano-impact testing was performed on PSZ and alumina with a NanoTest fitted with two different indenter geometries (a cube-corner diamond and a 5- μm end-radius diamond). The energy supplied per impact is the product of the impact load and the accelerating distance. The indenter was accelerated from 20 μm above the surface with 2–50 mN impact load to produce an impact every 4 s for 300 s (75 impacts). The applied loads were 2 mN and 5 mN for the cube-corner probe and 5 mN and 50 mN for the spheroconical probe. The resistance to impact fatigue was assessed by following the progression of the impact depth with continued impacts. The repetitive nano-impact test results were dependent on the probe geometry and applied load. Both ceramics showed a brittle response with progressive deformation and, in some cases, abrupt displacement bursts. AE monitoring was able to show that they were due to cracking rather than slip. An example of alumina with a cube-corner indenter at 5 mN is shown in Fig. 6a.

With the sphero-conical probe, the results were strongly dependent on the applied load. With the low load of 5 mN, there were very few impact events and a low final depth, but in the 50-mN tests, there was a transition to a situation where almost every impact resulted in cracking. This is illustrated in Fig. 6b, which shows the results of 5 impact tests superimposed on the same graph and the corresponding AE record. In general, the strongest AE signal correlates well with the regions of gradually increasing depth, where intensive cohesive damage of PSZ occurs.

CONCLUSION

Acoustic emission monitoring is a very useful technique and a rich source of unique information at the nano- and micro-scales. Implementation of AE to nanomechanical tests such as nano-indentation, scratch and nano-impact tests can significantly improve the reliability of conclusions drawn about the material mechanical durability and tribological performance. Due to its high sensitivity, various fracture- and yield-related phenomena can be

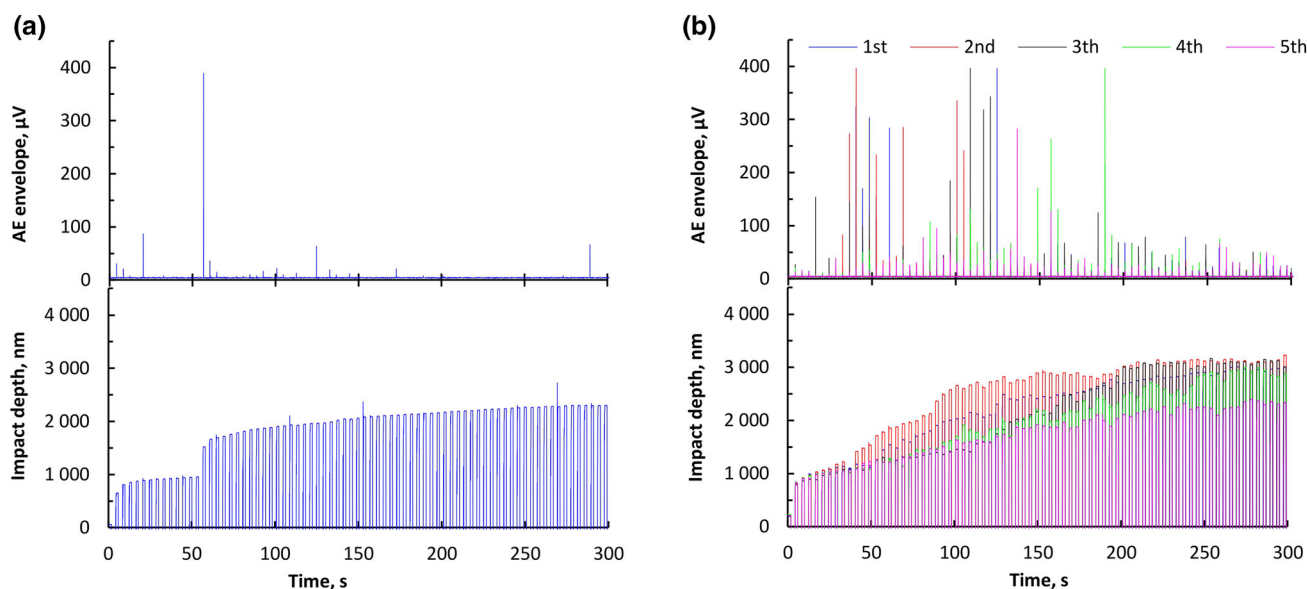


Fig. 6. AE records and impact depths for nano-impact tests performed (a) at 5 mN on alumina with a cube-corner indenter and (b) at 50 mN on PSZ with a 5- μm spherical indenter.

explored, as outlined in this paper. AE coupled with nanomechanical tests enables the detection of the very first sub-surface cohesive and/or adhesive failures, as well as the fundamental processes governing plastic deformation that are inaccessible by other methods.

The AE technique can be easily implemented in almost any mechanical and tribological test system and can be explored in time and frequency domains at different levels. Basic evaluation of AE signals can be made based on analysis of the AE envelope and its correlation to load–depth–time records or microscopic images of residual indents, scratches or craters. Deeper AE data evaluation may be performed by studying of individual AE hit parameters representing individual localized events. Although AE data are largely dependent on the experimental equipment and setup, their utilization opens a new way of how to readily obtain unique information and improve the conclusions about the material behavior.

ACKNOWLEDGEMENTS

The authors gratefully acknowledge the support by the Project TH03020245 of the Technology Agency of the Czech Republic and the Operational Programme Research, Development and Education, Projects Nos. CZ.02.1.01/0.0/0.0/17_049/0008422 and CZ.02.1.01/0.0/0.0/16_019/0000754 of the Ministry of Education, Youth and Sports of the Czech Republic.

REFERENCES

- R. Ctvrtlik, M. Al-Haik, and V. Kulikovskiy, *J. Mater. Sci.* 50, 1553 (2015).
- N.H. Faisal, R. Ahmed, and R.L. Reuben, *Int. Mater. Rev.* 56, 98 (2011).
- A. Vinogradov, A.V. Danyuk, D.L. Merson, and I.S. Yasniov, *Scr. Mater.* 151, 53 (2018).
- N.H. Faisal, R.L. Reuben, and R. Ahmed, *Meas. Sci. Technol.* 22, 015703 (2010).
- D.E. Kramer, K.B. Yoder, and W.W. Gerberich, *Philos. Mag.* A 81, 2033 (2001).
- P. Dyjak and R.P. Singh, *Exp. Mech.* 46, 333 (2006).
- D.F. Bahr and W.W. Gerberich, *J. Mater. Res.* 13, 1065 (1998).
- S.K. Lawrence, D.F. Bahr, and H.M. Zbib, *J. Mater. Res.* 27, 3058 (2012).
- C.-K. Lin and C.C. Berndt, *Surf. Coat. Technol.* 102, 1 (1998).
- X. Li, *Int. J. Mach. Tool Manuf.* 42, 157 (2002).
- M. Shiwa, E. Weppelmann, D. Munz, M.V. Swain, and T. Kishi, *J. Mater. Sci.* 31, 5985 (1994).
- N. Ali, Q. Hua Fan, J. Grácio, E. Pereira, and W. Ahmed, *Thin Solid Films* 377-378, 193 (2000).
- N.I. Tymiak, A. Daugela, T.J. Wyrobek, and O.L. Warren, *J. Mater. Res.* 18, 784 (2003).
- J. Tomastik, R. Ctvrtlik, M. Drab, and J. Manak, *Coatings* 8, 196 (2018).
- J. Tomastik, R. Ctvrtlik, T. Ingr, J. Manak, and A. Opletalova, *Sci. Rep.* 8, 10428 (2018).
- V. Perflyev, I. Lapsker, A. Laikhtman, and L. Rapoport, *Tribol. Lett.* 65, 24 (2017).
- V. Perflyev, A. Moshkovich, I. Lapsker, and L. Rapoport, *Tribol. Lett.* 65, 41 (2017).
- Á.I. Hegyi, P.D. Ispánovity, M. Knappek, D. Tüzes, K. Máthias, F. Chmelík, Z. Dankházi, G. Varga, and I. Groma, *Microsc. Microanal.* 23, 1076 (2017).
- A.C. Fischer-Cripps, *Nanoindentation* (Berlin: Springer, 2004).
- W.W. Gerberich, S.K. Venkataraman, H. Huang, S.E. Harvey, and D.L. Kohlstedt, *Acta Metall. Mater.* 43, 1569 (1995).
- N.Q. Chinh, J. Gubicza, Z. Kovács, and J. Lendvai, *J. Mater. Res.* 19, 31 (2011).
- D.F. Bahr, D.E. Kramer, and W.W. Gerberich, *Acta Mater.* 46, 3605 (1998).
- A. Gouldstone, H.J. Koh, K.Y. Zeng, A.E. Giannakopoulos, and S. Suresh, *Acta Mater.* 48, 2277 (2000).
- C.A. Schuh, A.C. Lund, and T.G. Nieh, *Acta Mater.* 52, 5879 (2004).
- S. Suresh, T.G. Nieh, and B.W. Choi, *Scr. Mater.* 41, 951 (1999).

26. T. Zhu and J. Li, *Prog. Mater. Sci.* 55, 710 (2010).
27. N. Gane and F.P. Bowden, *J. Appl. Phys.* 39, 1432 (1968).
28. B.D. Beake and S. Goel, *Int. J. Refract. Met. Hard Mater.* 75, 63 (2018).
29. K.L. Johnson, *Contact mechanics* (Cambridge: Cambridge University Press, 1985).
30. H. Hertz, *Mathematik* 92, 146 (1881).
31. C.A. Schuh and A.C. Lund, *J. Mater. Res.* 19, 2152 (2004).
32. L. Brabec, P. Bohac, M. Stranyanek, R. Ctvrtilik, and M. Kocirik, *Microporous Mesoporous Mater.* 94, 226 (2006).
33. T.C.T. Pham, H.S. Kim, and K.B. Yoon, *Science* 334, 1533 (2011).
34. A. Tavoraro and E. Drioli, *Adv. Mater.* 11, 975 (1999).
35. H.A. Kubavat, J. Shur, G. Ruecroft, D. Hipkiss, and R. Price, *Pharm. Res.* 29, 994 (2012).
36. S. Zügner, K. Marquardt, and I. Zimmermann, *Eur. J. Pharm. Biopharm.* 62, 194 (2006).
37. B.R. Lawn and M.V. Swain, *J. Mater. Sci.* 10, 113 (1975).
38. K. Holmberg, H. Ronkainen, and A. Matthews, *Ceram. Int.* 26, 787 (2000).
39. S.J. Bull, *Surf. Coat. Technol.* 50, 25 (1991).
40. N. Schwarzer, Q.H. Duong, N. Bierwisch, G. Favaro, M. Fuchs, P. Kempe, B. Widrig, and J. Ramm, *Surf. Coat. Technol.* 206, 1327 (2011).
41. J. Valli, U. Makela, A. Matthews, and V. Murawa, *J. Vac. Sci. Technol. A* A3, 2411 (1985).
42. H. Jensen, U.M. Jensen, and G. Sorensen, *Surf. Coat. Technol.* 74–75, 781 (1995).
43. J. Griffin and X. Chen, *Int. J. Nanomanuf.* 1, 189 (2006).
44. C. Leone, G. Caprino, and I. de Iorio, *Compos. Sci. Technol.* 66, 233 (2006).
45. B.D. Beake, L. Isern, J.L. Endrino, and G.S. Fox-Rabinovich, *Wear* 418–419, 102 (2019).
46. B.D. Beake, J.F. Smith, A. Gray, G.S. Fox-Rabinovich, S.C. Veldhuis, and J.L. Endrino, *Surf. Coat. Technol.* 201, 4585 (2007).

Publisher's Note Springer Nature remains neutral with regard to jurisdictional claims in published maps and institutional affiliations.